CHEMISTRY OF MATERIALS
Article

Chem. Mater. **2010,** *22,* 3653–3663 3653
DOI:10.1021/cm903596q

In Vivo Inspired Conditions to Synthesize Biomimetic Hydroxyapatite

N. Nassif,*,† F. Martineau,† O. Syzgantseva,† F. Gobeaux,† M. Willinger,‡ T. Coradin,† S. Cassaignon,† T. Azaïs,† and M. M. Giraud-Guille†

†*Laboratoire Chimie de la Matière Condensée de Paris, UMR 7574 CNRS, Université Pierre et Marie Curie, Collège de France, 11 place Marcelin Berthelot, 75231 Paris cedex 05, France, and* ‡*Department of Chemistry, CICECO, University of Aveiro, 3810-193 Aveiro, Portugal*

Received November 27, 2009. Revised Manuscript Received March 8, 2010

We present a simple one-pot crystallization method, inspired by biological conditions, for the synthesis of hydroxyapatite ($Ca_5(PO_4)_3OH$) nanocrystals. The reaction proceeds via NH_3 vapor diffusion into a $CaCl_2-NaH_2PO_4$ mixed solution that is free of any organic additives. The advantage of relying on acidic calcium-phosphate precursors here is, first, that the reaction can be performed at room temperature within a short time and without direct pH control and, second, that it does not produce any secondary phases or byproduct. Furthermore, the addition of $NaHCO_3$ to the salt solution or the introduction of $(NH_4)_2CO_3$ instead of NH_3 lead, respectively, to the precipitation of B- or A-type carbonate-apatite phases according to the FT-IR data. Multinuclear solid state NMR studies and especially ^{13}C CP experiments allow an in-depth characterization showing the presence of A/B substitutions in carbonated samples as well and indicate a close similarity to deproteinated bovine compact bone. A precipitation mechanism accounting for the precipitation of mainly A- or B-type carbonated apatite under the respective experimental conditions is proposed.

1. Introduction

Calcium phosphates (Ca-Pi's) are important mineral phases due to their significance as biominerals and their various industrial and medical applications.[1] In living organisms, Ca-Pi phases are mainly present in bone, cartilage, dentin, and enamel as substituted hydroxyapatite (HA, ($Ca_5(PO_4)_3OH$)). The control of crystallization over several length scales in these biomineralization processes has been extensively studied.[2] The structure and chemical composition of the Ca-Pi solid phase in biological systems are difficult to define accurately, mainly because tissues such as bone are constantly being renewed and remodeled. Ca-Pi in young bone substance has been characterized as very thin plate-like nanocrystals of substituted apatite. With time, it gradually contains a higher percentages of pure crystalline hydroxyapatite.[3]

The design of composite or hybrid organic/inorganic materials in bone tissue engineering requires biocompatible mineralization processes. This is particularly true in the presence of bio-organic components, namely, collagen, the main structural macromolecule of bone. Indeed, this protein is irreversibly denaturated into gelatin when heated *in vitro* even at low temperature.[4] Additionally, since the HA properties such as crystallinity, thermal stability, and solubility have been shown to be dependent on the fabrication route,[5] in a biomimetic approach, one has to find a route taking both organic/inorganic properties into account, at least via aqueous precipitation and in relatively mild temperature conditions.[6]

Several methods that rely on an acid−base reaction at constant calcium-phosphate composition have already been reported, for instance, $H_3PO_4/Ca(OH)_2$[5,7,8] and $(NH_4)_2HPO_4/CaNO_3$[8−10] systems. They are mainly carried out with an alkaline or a slightly acidic (at least pH > 5) starting pH. By doing so, they avoid the formation of other calcium-phosphate phases, in particular brushite ($CaHPO_4 \cdot 2H_2O$), which is the stable phase below pH 4.2.[11,12] Moreover, further introduction of a CO_2 flux has opened up a route for the synthesis of carbonate-substituted hydroxyapatite (CHA) powders.[13] However, these methods require a careful identification and control of parameters (dropwise addition, nature and

*Corresponding author. E-mail: nadine.nassif@upmc.fr.

(1) Rey, C. Calcium Phosphates for Medical Applications. *Calcium Phosphates in Biological and Industrial Systems*; Amjad, Z., Ed.; Kluwer Academic Publishers: Boston, MA, 1998; pp 217−251.
(2) Mann, S. *Biomineralization: Principles and Concepts in Bioinorganic Materials Chemistry*; Oxford Chemistry Masters; Oxford University Press: Oxford, U.K., 2001.
(3) Glimcher, M. J. *Rev. Mineral. Geochem.* **2006**, *64*, 223–282.
(4) Shnyrov, V. L.; Lubsandorzhieva, V. C.; Zhadan, G. G.; Permyakov, E. A. *Biochem. Int.* **1992**, *26*, 211–217.
(5) Bernard, L.; Freche, M.; Lacout, J. L.; Biscans, B. *Powder Technol.* **1999**, *103*, 19–25.
(6) Ferraz, M. P.; Monteiro, F. J.; Manuel, C. M. *J. Appl. Biomater. Biomech.* **2004**, *2*, 74–80.
(7) Osaka, A.; Miuri, Y.; Takeuchi, K.; Asada, M.; Takahashi, K. *J. Mater. Sci.: Mater. Med.* **1991**, *2*, 51–55.
(8) Verwilghen, C.; Rio, S.; Nzihou, A.; Gauthier, D.; Flamant, G.; Sharrock, P. J. *J. Mater. Sci.* **2007**, *42*, 6062–6066.
(9) Jarcho, M.; Bolen, C. H. *J. Mater. Sci.* **1976**, *11*, 2027–2035.
(10) Hayek, E.; Newesely, H. *Inorg. Synth.* **1963**, *7*, 63–65.
(11) Ferreira, A.; Oliveira, C.; Rocha, F. *J. Cryst. Growth* **2003**, *252*, 599–611.
(12) De Rooij, J. F.; Heughebaert, J. C.; Nancollas, G. H. J. *Colloids Interface Sci.* **1984**, *100*, 350–358.
(13) Celotti, G.; Landi, E.; Sandri, M.; Tampieri, A. *Key Eng. Mater.* **2004**, *264−268*, 2071–2074.

Published on Web 05/18/2010

composition of the starting components, pH, temperature) to obtain a pure single apatite phase. Moreover, if precipitation occurs at room temperature, heating is required for phase transformation of kinetic intermediates into stable apatite and/or to get rid of the reaction byproduct. In fact, only a few methods have been entirely set at room-to-physiological temperature, for example, the double diffusion technique[14] or the impregnation in simulated body fluid (SBF).[15−17] A drawback of the double diffusion method is the formation of relatively stable brushite together with HA crystals. The SBF used as a reservoir of ions has the strong advantage of being the closest to physiological conditions. However, the preparation of the metastable solution is a tedious procedure which increases the risk of obtaining nonreproducible results.[18] As a last example, the synthesis of bone-like nanocrystalline hydroxyapatite was proposed by using amorphous calcium-phosphate precursors. However, this approach needs a continuous computer-controlled reactor.[19]

The present work is based on the idea that *in vitro* synthesis of biomimetic apatite can be set by using simple chemical conditions occurring *in vivo*. In bone tissue, osteoclasts degrade bone matrix in an acidic extracellular compartment; therefore, apatite precursor species building the new bone mineral phase are recycled starting from low pH. In contrast to aqueous hydroxyapatite precipitations in the literature, we have used apatite precursors at low pH. A simple aqueous one-pot precipitation method is proposed through a variant of the vapor diffusion technique which is popular for slow $CaCO_3$ crystallization as it enables the synthesis of the calcite thermodynamic phase.[20] The crystallization method for HA is performed via vapor diffusion of ammonia (NH_3) into an acidic calcium-phosphate ($CaCl_2-NaH_2PO_4$) solution based on thermodynamic conditions to avoid the precipitation of other calcium-phosphate phases. Thus, this precipitation method, which is free of any organic additives, has the advantage of being conducted at room temperature within a few hours, without direct pH control, and does not produce any byproduct or contaminated phases. The interest in this process is further demonstrated by showing that the sole modification of the nature of the carbonate precursor allows the orientation of the synthesis toward mainly A- or B-type carbonate substituted HA phases. The nature and structure of the resulting materials are studied by X-ray diffraction, FT-IR, and multinuclear (^1H, ^{31}P, and ^{13}C) solid state NMR. ^{13}C CP MAS experiments are shown to be particularly useful to investigate in more detail the carbonated samples. In particular, in contrast to FT-IR results, these measurements evidence a more complex chemical environment for carbonate anions, i.e., combination of A/B-type sites, in the synthetic materials that is similar to the one in deproteinated bovine compact bone. Finally, we propose a precipitation mechanism based on the nature and reactivity of inorganic precursors that correlates the modification of the experimental conditions with the formation of preferentially A- or B-type carbonated hydroxyapatite.

Table 1. Concentrations of Salt Precursors Used in HA Synthesis

	aqueous NH_3		solid $(NH_4)_2CO_3$	
precursors	molarity (mM)			
$CaCl_2.2H_2O$	110	110	110	110
NaH_2PO_4	66	33	66	33
$NaHCO_3$		33		33
	HA-1	HA-2	HA-3	HA-4

Scheme 1. Schematic of Vapor Diffusion Processes in HA Precipitation[a]

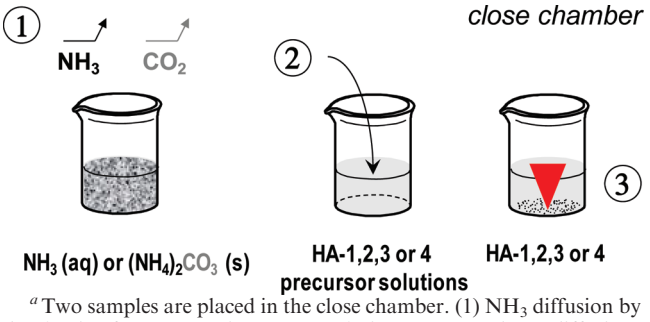

[a] Two samples are placed in the close chamber. (1) NH_3 diffusion by desolvation from ammonia aqueous solution or NH_3 and CO_2 diffusions by decomposition of solid ammonium carbonate; (2) solubilization (NH_3, CO_2) and diffusion into the acidic HA-1,2,3, or 4 precursor solutions; (3) HA-1,2,3, or 4 precipitations.

2. Experimental Section

Experiments were carried out at room temperature (22 ± 1 °C). Two solutions were prepared in acetic acid (500 mM): (i) a $CaCl_2/NaH_2PO_4$ solution with a calcium-to-phosphate (Ca/P) molar ratio of 1.67, consistent with the formation of HA with a formula of $Ca_{10}(PO_4)_6(OH)_2$ and (ii) a $CaCl_2/NaH_2PO_4/NaHCO_3$ solution with a calcium-to-phosphate plus carbonate (Ca/[P + C]) molar ratio of 1.67, consistent with the formation of CHA with a formula of $Ca_{10-x}(PO_4)_{6-x}(CO_3)_x(OH)_{2-x}$ with $0 \le x \le 2$. The pH was then adjusted to 2.2. The concentrations of precursors are detailed in Table 1. Two flasks (35 mL, h = 50 mm) separately containing one of those solutions (20 mL) covered by perforated Parafilm (to slow down the gas diffusion) were placed into a closed chamber (1000 cm^3). The HA precipitation was triggered via the slow increase of the pH of the solution induced by the introduction of fresh ammonia aqueous solution (30% w/w, 8 mL) or solid ammonium carbonate $(NH_4)_2CO_3$ (4 g) in the chamber. The technique is summarized in Scheme 1. Addition of different concentrations of $CaCl_2$ was studied (11, 55, and 110 mM). However, as these variations only affected the amount of precipitated materials and not their nature or structure, the highest concentration was used. A few hours after ammonia or ammonium carbonate introduction, precipitation occurs in the solution. After complete gas diffusion (pH ∼10), the solids were washed and centrifuged (6000 rpm,

(14) Peytcheva, A.; Cölfen, H.; Schnablegger, H.; Antonietti, M. *Colloid Polym. Sci.* **2002**, *280*, 218–227.
(15) Kokubo, T.; Takadama, H. *Biomaterials* **2006**, *27*, 2907–2915.
(16) Zhang, L. J.; Feng, X. S.; Liu, H. G.; Qian, D. -J.; Zhang, L.; Yu, X. L.; Cui, F.-Z. *Mater. Lett.* **2004**, *58*, 719–722.
(17) Schwarz, K.; Epple, M. *Chem.—Eur. J.* **1998**, *4*, 1898–1903.
(18) Bohner, M.; Lemaitre, J. *Biomaterials* **2009**, *30*, 2175–2179.
(19) Tadic, D.; Peters, F.; Epple, M. *Biomaterials* **2002**, *23*, 2553–2559.
(20) Addadi, L.; Moradian, J.; Shay, E.; Maroudas, N. G.; Weiner, S. *Proc. Natl. Acad. Sci. U.S.A.* **1987**, *84*, 2732–2736.

10 min) first in distilled water and then in ethanol in order to remove the nonprecipitated salts. The recovered crystals were dried at 37 °C before characterization.

The organic matrix (collagen and other proteins) was removed from compact and trabecular mature bovine bone by a NaOH aqueous solution (1 M) treatment. The bone samples were stirred at room temperature in the alkaline solution, which was renewed every 4 days, for 12 days until recovering a powder.

Powder X-ray diffraction (XRD) diagrams of all samples were performed on a Bruker D8 X-ray diffractometer operating in the reflection mode at CuKα radiation with 40 kV beam voltage and 40 mA beam current. The data were collected in the 10−50° range (2θ) with steps of 0.01° and a counting time of 9 s. JCPDS files were used to identify hydroxyapatite, HA (9−432), octacalcium phosphate OCP (44−778), and brushite, $CaHPO_4$, $2H_2O$, DCPD (11−293). Transmission electron microscopy (TEM) investigations were performed on a Philips CM12 electron microscope, operated at 120 kV and equipped with a CDD camera. High resolution TEM was performed using a Philips CM200 with a field emission gun and a postcolumn GATAN Tridiem image filter. The microscope was operated at 200 kV. For TEM investigations, samples were prepared by evaporating a drop of ethanol diluted suspension on a carbon-coated copper grid. Fourier-transform infrared spectroscopy FT-IR was performed on a Nicolet Magna FT-IR spectrometer. Samples coated with gold were studied by scanning electron microscopy (SEM) using a JEOL model JSM-5510 LV at an accelerating voltage of 10 kV. ^1H, ^{31}P, and ^{13}C solid state NMR experiments were performed on an Avance 300 Bruker spectrometer operating at $\nu(^1H) = 300.13$ MHz, $\nu(^{31}P) = 121.50$ MHz, and $\nu(^{13}C) = 75.48$ MHz using a double channel 4 mm probe. ^{31}P single pulse MAS spectra were acquired at a MAS frequency (ν_{MAS}) of 14 kHz with a recycle delay (RD) of 300 s according to $T_1(^{31}P)$ measurements assuring quantitative measurements. ^1H single pulse MAS spectra were acquired at $\nu_{MAS} = 14$ kHz with RD = 2 s according to $T_1(^1H)$ measurements and assuring quantitative measurements in the same manner as that used in ^{31}P experiments. 2D ^1H spin diffusion experiments were carried out using the standard exchange spectroscopy EXSY experiments[21,22] with a mixing time of 100 ms and with RD = 2 s at $\nu_{MAS} = 14$ kHz. ^{13}C CP MAS spectra were acquired at $\nu_{MAS} = 5.5$ kHz (RD = 2 s) using a ramp CP[23] with a contact time t_{CP} of 5 ms. The number of scans, NS, comprised between 30000 and 80000. ^{31}P and ^{13}C experiments were recorded with TPPM ^1H high power decoupling during acquisition.[24] The Hartmann−Hahn condition was set on adamantane. The chemical shift reference (0 ppm) was tetramethylsilane (TMS) for ^1H and ^{13}C, and 85% aqueous H_3PO_4 for ^{31}P.

3. Results and Discussion

Synthesis and Structural Characterization. Calcium phosphate precipitations were carried out either with ammonia solution (HA-1 and HA-2) or with solid ammonium carbonate (HA-3 and HA-4). The critical pH required for the precipitation of HA is reached by vapor diffusion and dissolution of ammonia into the Ca−P mixed solution. The decomposition of solid ammonium carbonate additionally provides the source of carbonate in the system as it releases both NH_3 and CO_2 vapors. Sodium bicarbonate ($NaHCO_3$) is added as an alternative (HA-2) or an additional (HA-4) source of carbonate ions. The precursor concentrations of the two different solutions were set to Ca/P and Ca/(P + C) molar ratio of 1.67, which is consistent with the formation of HA and CHA, respectively.

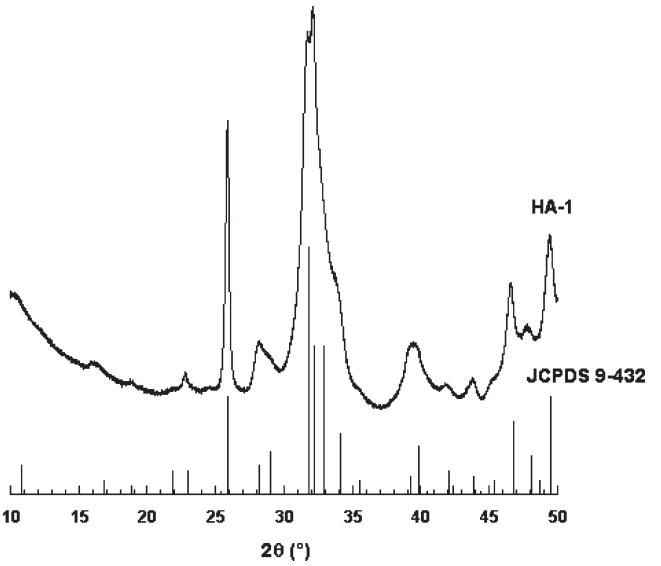

Figure 1. X-ray diffraction patterns of synthetic hydroxyapatite synthesized via the vapor diffusion process (HA-1) and extracted from the literature.

The phase identification of the resulting materials was carried out by X-ray powder diffraction (XRD) analysis (see HA-1 in Figure 1 and HA-2 HA-3 in Supporting Information Figure 1). X-ray diffraction patterns were similar for all samples and show the formation of the thermodynamically stable hydroxyapatite which occurred in a matter of hours. According to JCPDS file number 9-432, the main diffraction peaks in 2θ could be assigned to the HA (hkl) indices as follows: 25.9° (002); 31.8°, 32.2°, and 32.9° included in the broad region of overlapping peaks corresponding to (211), (112), and (300), respectively; 34.1° (202); 39.8° (310); and 46.7° (222). The absence of octacalcium phosphate (OCP) as an intermediary phase could be ascertained since its main diffraction peak (100) expected at 4.7° was not observed. However, it is often reported that in the early stages of *in vitro* reactions, amorphous calcium-phosphate (ACP), $Ca_3(PO_4)_2 \cdot nH_2O$ particles, are formed,[25] which subsequently transform into hydroxyapatite. The process is described to be faster with a Ca/P molar ratio of 1.76 and at 37 °C.[26] In the present system, the presence of ACP cannot be put aside since its broad reflection could be hidden by the crystalline apatite peak; but its amount

(21) Jeener, J.; Meier, B. H.; Bachmann, P.; Ernst, R. R. *J. Chem. Phys.* **1979**, *71*, 4546–4553.
(22) Schmidt-Rohr, K.; Spiess, H. W. *Multidimensional Solid-State NMR and Polymers*; Academic Press: London, 1994.
(23) Peersen, O. B.; Wu, X.; Kustanovich, I.; Smith, S. O. *J. Magn. Reson., Ser. A* **1993**, *104*, 334–339.
(24) Bennett, A. E.; Rienstra, C. M.; Auger, M.; Lakshmi, K. V.; Griffin, R. G. *J. Chem. Phys.* **1995**, *103*, 6951–6958.
(25) Eanes, E. D.; Gillesen, I. H.; Posner, A. S. *Nature* **1965**, *208*, 365–367.
(26) Gibson, I. R.; Best, S. M.; Bonfield, W. *J. Biomed. Mater. Res.* **1999**, *44*, 422–428.

would then be relatively small. Overall, the XRD powder pattern displays broad peaks indicating the presence of nanocrystalline HA[19] similar to that of HA crystals present in embryonic chick bone[27] and comparable with mature trabecular and compact bovine bone (see Supporting Information, Figure 1). This could be explained by the fact that the synthesis of HA is performed in aqueous solution and at room temperature. The relatively high intensity of the 002 reflection seems to indicate a preferential orientation of the ground HA crystals on the sample holder. It is also very likely that the nanoparticles are already preferentially oriented almost orthogonal to the gas diffusion surface in the solution. Similar conclusions were proposed for continuous carbonated hydroxyapatite film grown using the stearic acid monolayer as a template.[28] The average crystallite size of 50 nm in the (002) direction (*c* axis), determined using Scherrer's equation and the fwhm[29] of the corresponding peak (25.9°), is in the same range as the one found in natural bone nanocrystals (see Supporting Information, Figure 1).

In contrast to the cases of HA-1, -2, and -3, the experimental conditions for HA-4 lead to the additional formation of rhombohedral calcite ($CaCO_3$) crystals. The presence of calcite was confirmed by SEM (see Supporting Information, Figure 2a) and XRD data (diffraction peaks 2θ (hkl): 29.27 (104), 39.42 (202), 47.36 (018) in Supporting Information, Figure 2b) and is certainly due to a higher content of HCO_3^-, resulting from the concomitance of the two carbonate sources, i.e., solid ammonium carbonate and sodium bicarbonate. Interestingly, calcium carbonate is also found in bone *in vivo*,[30] and therefore, the present experimental conditions and setup could constitute an alternative procedure to precipitate such mixed phases *in vitro*. However, the following characterizations will be focused on HA-1, -2, and -3 samples where only one phase is obtained.

Morphological and Chemical Characterization. Scanning electron microscopy (SEM) observations reveal the high uniformity of the synthesized materials (Figure 2a). At higher magnification, flower-like spherulitic aggregates with a diameter of around 5 μm (Figure 2b) can be observed. Similar HA morphologies were obtained previously by precipitation of SBF on alkali-treated titanium[31] or with calcium-phosphate solution in the presence of ureases.[32]

Observations of the samples using transmission electron microscopy (TEM) demonstrate that the spherulitic agglomerates consist of very thin leaves of bent and flat platelets (see Figure 3a, inset Figure 3b, and Figure 3c). Besides the thin sheets, some rod-like structures are visible. From their morphology, it appears that some of these rod-like structures either correspond to thin sheets that have folded up or to sheets that are viewed from the side (see Figure 4). The observation of continuous lattice fringes across individual platelets in high resolution TEM (HRTEM) proves that the platelets are single crystalline in nature (see Figure 3b and d). Spacing and angles of the lattice fringes can consistently be assigned to the structure of hydroxyapatite. They reveal that the platelets grow along the [001] direction while generally exposing the (100) faces. The same growth direction was found for the rod-like structures mentioned above. This explains the high intensity of the 002 reflection in the XRD diagram. As exemplified in Figure 3, the lattice fringes generally extend to the border of the platelets. Hence, no amorphous surface layers were detected. Overall, the crystallinity is very good, and no indication for ACP was found. Morphologically, no obvious differences between HA-1 and HA-2 could be detected by electron microscopy. The dimension of individual particles confirms the above XRD data and is reminiscent of the bone nanocrystal shape.[27,33] Indeed, for comparison,

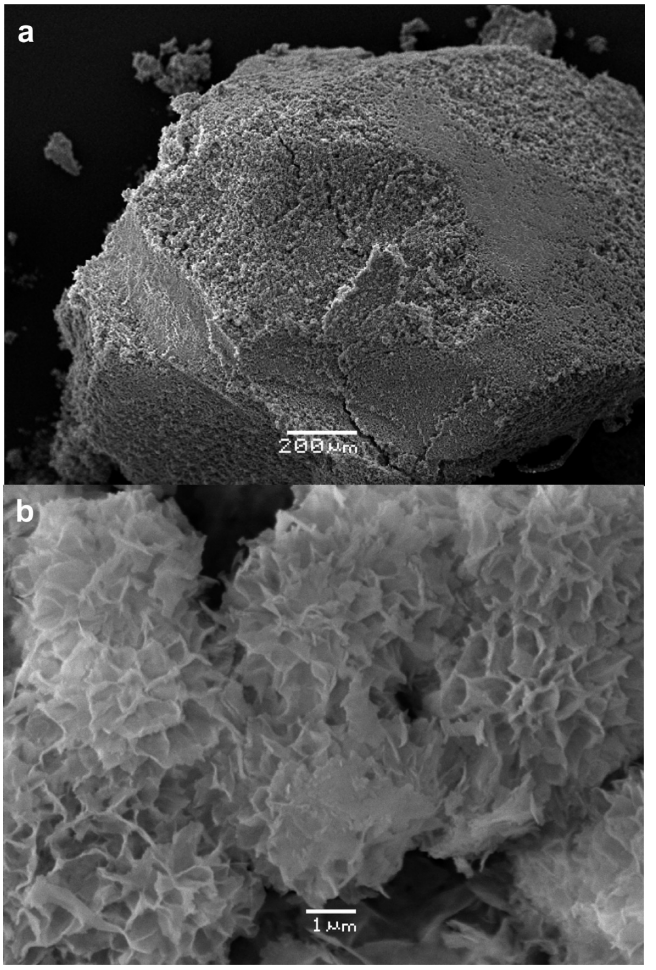

Figure 2. SEM (a) overview image showing a dense agglomeration of particles and (b) revealing, at higher magnification, individual flower-like spherulitic aggregates in the HA-2 sample.

(27) Kim, H. M.; Rey, C.; Glimcher, M. J. *J. Bone Miner. Res.* **1995**, *10*, 1589–1601.
(28) Boanini, E.; Bigi, A. *Thin Solid Films* **2006**, *497*, 53–57.
(29) Suryanarayana, C.; Grant Norton, M. *X-ray Diffraction. A Practical Approach*; Plenum Press: New York, 1998.
(30) Pellegrino, E. D.; Biltz, R. M. *Calc. Tiss. Res.* **1970**, *6*, 168–171.
(31) Müller, L.; Müller, F. A. *Acta Biomater.* **2006**, *2*, 181–189.
(32) Ortega, I.; Jobbagy, M.; Ferrer, M. L.; Del Monte, F. *Chem. Mater.* **2008**, *20*, 7368–7370.
(33) Landis, W. J.; Moradian-Oldak, J.; Weiner, S. *Connect. Tissue Res.* **1991**, *25*, 181–196.

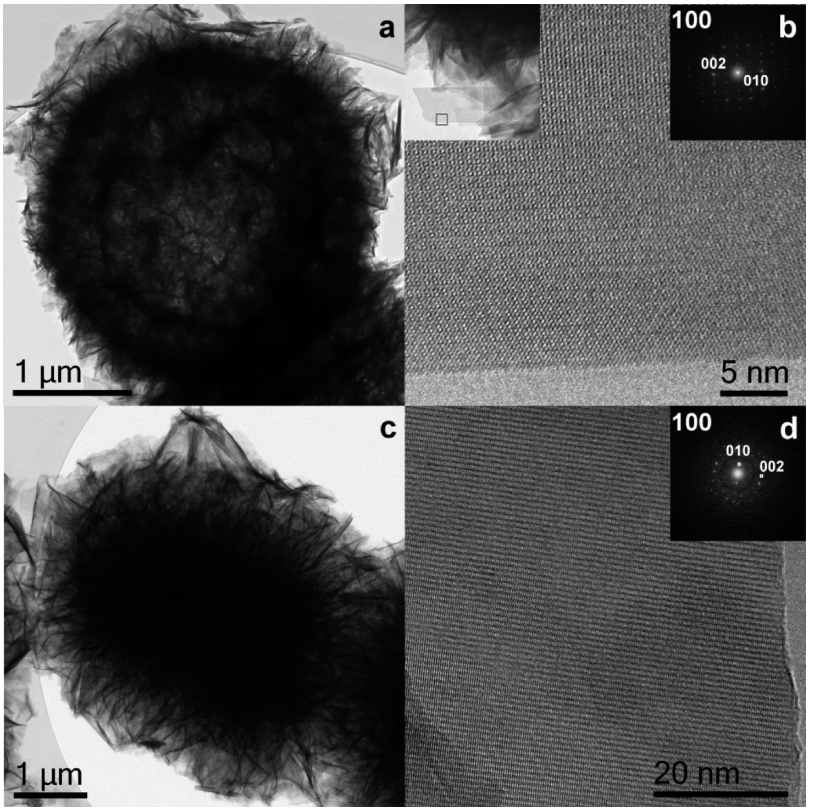

Figure 3. (Left) TEM Overview images showing spherical aggregates of thin platelets in HA-1 (a) and HA-2 (c). Some of the thin sheets are strongly bent or folded. (Right) HRTEM images and power spectra of single platelets revealing lattice fringes that correspond to [100] oriented HA in HA-1 (b) and HA-2 (d). The growth direction of the platelets coincides with the [001] direction. The inset in b shows the region of a single platelet from which the high resolution image was recorded.

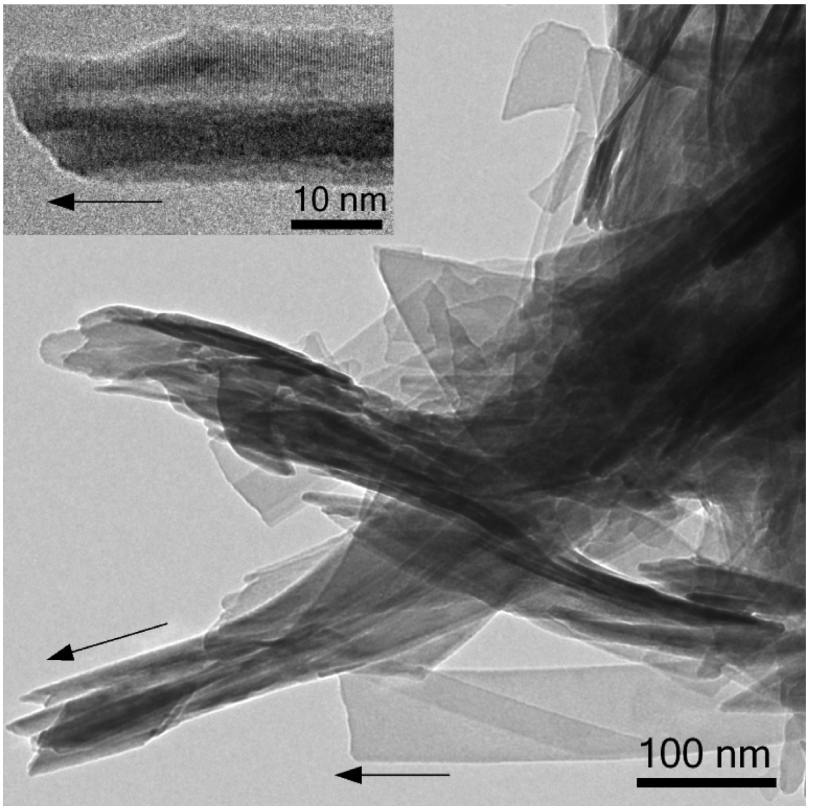

Figure 4. Folding of platelets gives rise to the appearance of rod-like structures. In transmission, platelets viewed from the side also appear as thin rods. The inset shows a higher magnified view of a rod with visible 002 lattice planes. Arrows indicate the [001] direction.

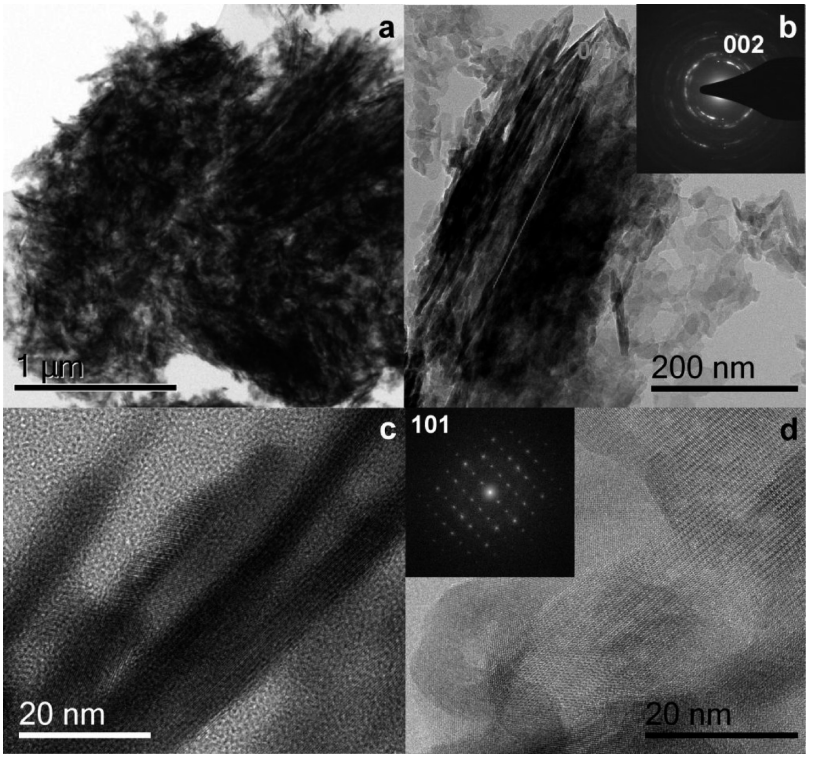

Figure 5. Agglomerations of HA particles in natural bone are shown in the top row (a,b). A bundle of rods and the corresponding SAED pattern are shown in (b). The alignment of the bright 002 spots in the SAED pattern with the long axis of the rods demonstrates their growth along the [001] direction. In the bottom row (c,d), HRTEM images of rods and platelets are shown. The power spectrum shown as an inset in d corresponds to [101] oriented HA.

deproteinated bovine compact bone was also investigated by TEM (see Figure 5). In agreement with the literature,[3] a growth direction along [001] was also found. It appears that the platelets that are found in the bone sample are less faceted with respect to those observed in HA-1 and HA-2. Additionally, the exposure of [100] planes appears to be less frequent in the natural bone. It remains reasonable to assume that it is due to the alkaline treatment performed to remove the organic matrix since stabilization of specific surfaces in bone apatite should be more enhanced than in our synthetic apatite free of organic additives, thus organic interactions. In addition, a higher portion of rod-like structures can be observed that are also growing along the [001] direction. This is demonstrated by the selected area diffraction pattern (SAED) shown as an inset in Figure 5. However, we would like to point out that drawing conclusions is notoriously difficult since such studies combine a procedure that affects the native tissue together with the intrinsic heterogeneity of bone.[3]

In order to quantify a possible carbonate substitution in these HA phases, elemental analysis was performed on samples after washing and drying at 37 °C. A good correlation between theoretical and experimental Ca/P molar ratios is found for all samples, with average values of 1.56, 1.73, and 1.58 for HA-1, HA-2, and HA-3, respectively. A low Ca/P molar ratio close to 1.5 is described in the literature for nanocrystalline HA[34] and is known to be optimal for the formation of ACP as well as tricalcium phosphate (TCP), $Ca_3(PO_4)_2$. However, in our conditions, XRD data did not indicate the presence of TCP.

The phase identification of the crystals was also confirmed by FT-IR spectroscopy (see Figure 6) that can more specifically discriminate between the formations of HA (see Figure 6a) and CHA (see Figures 6b and c) phases. For all spectra, similar vibrational bands are detected corresponding (i) to the PO_4 group at 472 (O−P−O bending ν_2), (ii) to the PO_4 group at 563 (O−P−O antisymmetric bending ν_4), 602 (O−P−O bending ν_4), 960 (P−O bending ν_1), and 1031−1120 (P−O bending ν_3) cm^{-1}, and (iii) to the presence of adsorbed water evidenced by the broad adsorption band at 3300−3600 cm^{-1}. As mentioned above, the presence of amorphous calcium-phosphate is suspected. The fact that the P−O bending ν_3 of HA-1 and HA-2 is better defined than for HA-3 could indicate a lower proportion of crystalline phase for the latter.[35] Additionally, in all spectra, a common band in the region of 1650 cm^{-1} indicates the presence of CO_3^{2-} adsorbed species remaining from the aqueous precipitation.[36]

Without any carbonate in the precipitation medium (HA-1 in Figure 6a), typical hydroxyapatite was formed as shown by the characteristic vibration band at 3570 cm^{-1} together with the weak intensity signal at 630 cm^{-1} corresponding to the librational mode of OH groups. We can notice the presence of weak bands in the 1400−1500 cm^{-1}

(34) Tadic, D.; Epple, M. *Biomaterials* **2003**, *24*, 4565–4571.

(35) Nawrot, C. F.; Campbell, D. J.; Schroeder, J. K.; Van Valkenburg, M. *Biochemistry* **1976**, *15*, 3445–3449.

(36) Kannan, S.; Lemos, A. F.; Ferreira, J. M. F. *Chem. Mater.* **2006**, *18*, 2181–2186.

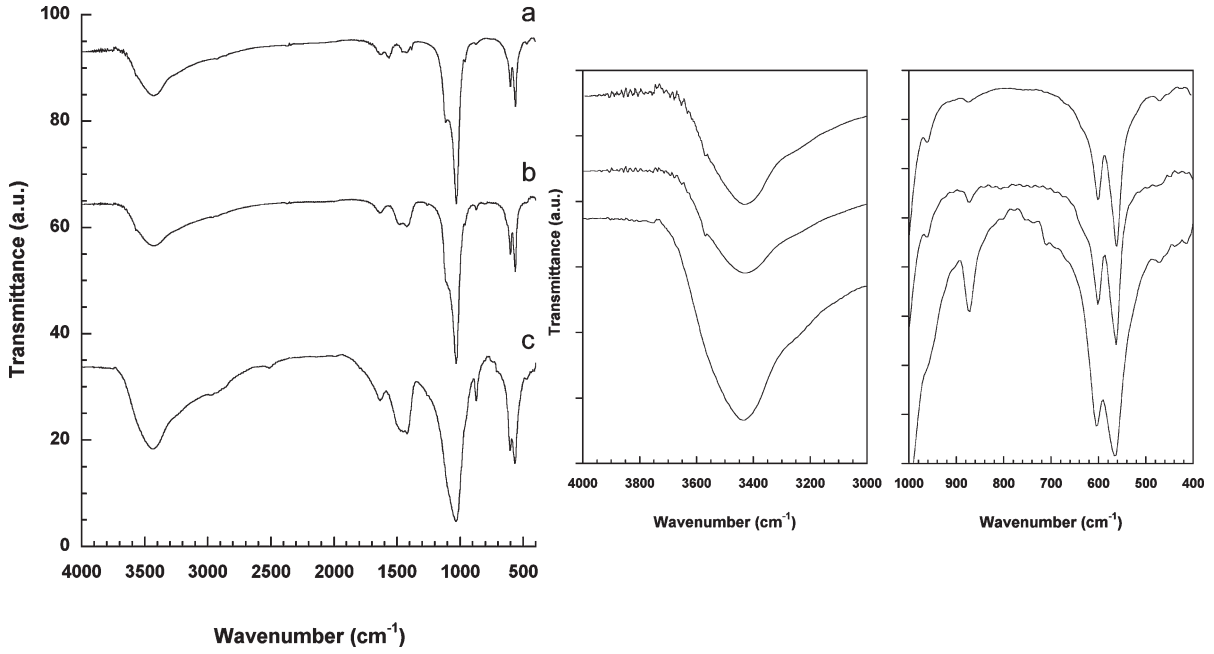

Figure 6. FT-IR spectra of (a) HA-1, (b) HA-2, and (c) HA-3.

region of the HA-1 sample suggesting the presence of carbonate ions which could originate from the dissolution of CO_2 from the atmosphere.[37]

Addition of sodium bicarbonate (HA-2 in Figure 6b) leads to the presence of absorption bands at approximately 1460−1420 cm^{-1}, which are consistent with the presence of carbonate ions. The fact that the vibration bands at 3570 cm^{-1} and 630 cm^{-1} of OH groups are still observable evidence a carbonated apatite classified as B-type (B-CHA) where CO_3^{2-} substitutes phosphate groups ($Ca_{10-x}(PO_4)_{6-x}(CO_3)_x(OH)_{2-x}$ with $0 \leq x \leq 2$).[38] This is in agreement with the literature showing that B-CHA is predominant in precipitation reactions.[39,40] Another characteristic vibration band is assigned to the CO_3^{2-} group of B-CHA at 872 cm^{-1} (see Figure 6b and Supporting Information, Figure 3b).[31] However, this band could also indicate either the presence of residual NH_4^+ ions[36,41] or HPO_4^{2-} incorporation into the structure as a shoulder is observed at 961 cm^{-1}.[31]

When ammonium carbonate constitutes the only carbonate source (HA-3 in Figure 6c), the previously mentioned absorption bands for CO_3^{2-} (1420 and 1460 cm^{-1}) are also observed. Moreover, the vibrational band at 3570 cm^{-1} disappears, and the band at 630 cm^{-1} has a weaker intensity compared to that of HA-2. Another characteristic vibration band is assigned to the CO_3^{2-} group of an A-type carbonate apatite (A-CHA) at 880 cm^{-1} (Supporting Information, Figure 3c).[42] Taken together, these data suggest the substitution of OH^- sites, rather than those of PO_4^{3-}, by carbonates (CO_3^{2-}), and thus the formation of an A-type carbonate apatite ($Ca_{10}(PO4)_6(OH)_{2-2y}(CO_3)_y$ with $0 \leq y \leq 1$ (A-type)).

As recently pointed out and illustrated above, characterization of carbonated apatite phases by FT-IR spectroscopy is not straightforward, as many bands originating from different species overlap, which can thus yield to ambiguous results.[43] It is even more pronounced when precipitation occurs at room temperature from aqueous solutions. Indeed, the crystalline domains are small compared to crystals obtained by high temperature processes, resulting in much broader bands. Thus, the ratio of A/B-type substitution, which can be estimated from the ratio of the intensities of the peaks at 880 and 873 cm^{-1}[44,45] is not easily accessed for our nanocrystalline samples. Moreover, the shoulder at 880 cm^{-1} could indicate HPO_4^{2-} incorporation into the structure as well.

Multinuclear NMR Characterization. Solid-state NMR is a useful tool used to characterize carbonated HA samples because of its capacity to probe the local environment for several nuclear spins.[46] If most of the HA NMR studies focused on ^1H and ^{31}P spectroscopy, ^{13}C NMR spectroscopy has been very rarely employed to probe the carbonate substitution both in synthetic and natural CHA samples, certainly due to the low amount of CO_3^{2-} present in the material (5−8 wt % in bone mineral for instance). To the best of our knowledge, only few studies have been performed with ^{13}C-labeled synthetic samples in order to propose an assignment of the characteristic resonances of A-, B-, and A/B-type

(37) Kumar, R.; Prakash, K. H.; Cheang, P.; Khor, K. A. *Langmuir* **2004**, *20*, 5196–5200.
(38) Elliott, J. C. *Structure and Chemistry of the Apatites and Other Calcium Orthophosphates*; Elsevier: The Netherlands, 1994.
(39) Nelson, D. G. A.; Featherstone, J. D. B. *Calcif. Tissue Int.* **1982**, *34*, 569–581.
(40) Barralet, J.; Knowles, J. C.; Best, S.; Bonfield, W. J. *J. Mater. Sci.: Mater. Med.* **2002**, *13*, 529–533.
(41) Raynaud, S; Champion, E.; Bernarche-Assolant, D.; Thomas, P. *Biomaterials* **2002**, *23*, 1065–1072.
(42) Lafon, J. P.; Champion, E.; Bernache-Assolant, D. *J. Eur. Ceram. Soc.* **2008**, *28*, 139–147.
(43) Fleet, M. E. *Biomaterials* **2009**, *30*, 1473–1481.
(44) Gibson, I. R.; Bonfield, W. *J. Biomed. Mater. Res.* **2002**, *59*, 697–708.
(45) Chang, M. C.; Tanaka, J. *Biomaterials* **2002**, *23*, 4811–4818.
(46) Kolodziejski, W. *Top. Curr. Chem.* **2004**, *246*, 235–270.

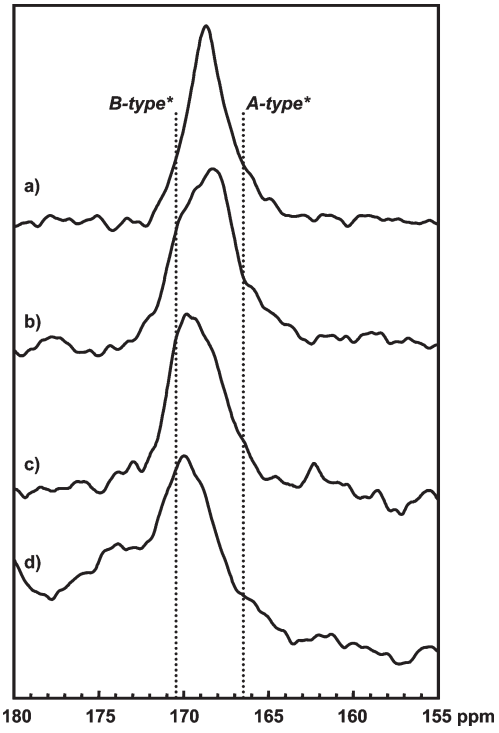

Figure 7. ^{13}C CP MAS spectra of (a) HA-3; (b) HA-2; and deproteinated (c) compact and (d) trabecular bone. *Dashed lines refer to the ^{13}C chemical shift of type-A and type-B carbonated hydroxyapatite according to refs 49 and 50.

carbonates.[47−49] Moreover, natural half-erupted enamel has been investigated by Beshah et al.,[47] and despite a poor signal-to-noise ratio (S/N), the major features of type-A and type-B resonances have been correlated with synthetic CHA.

^{13}C cross-polarization CP MAS NMR spectra were recorded with a contact time t_{CP} = 5 ms in a reasonable experimental time of 24−48 h despite the relatively low carbonate amount in the samples. The solid-state ^{13}C CP MAS spectra of HA-2 and HA-3 are depicted in Figure 7a,b. As expected, both samples present a resonance in the carbonate region. HA-2 exhibits an asymmetric resonance with a maximum at 168.4 ppm associated with a prominent shoulder at 170.1 ppm and a weaker one at 166.1 ppm (total fwhm = 4 ppm). HA-3 presents a sharper and nearly symmetric resonance centered at 168.8 ppm and associated with two weak shoulders at 170.6 and 166.2 ppm (total fwhm = 2.8 ppm). According to the literature data, resonances at 170.5 and 166.5 ppm can be assigned to B- and A-CHA, respectively.[47,48] On this basis, we can suggest that both samples are a mixture of A- and B-type CHA but with a larger ratio of B-type in HA-2 when compared to that of HA-3, supporting our previous conclusions. Furthermore, considering that the spectra were acquired using the CP process where the ^{1}H spin magnetization is transferred to ^{13}C nuclei, A-type carbonate ^{13}C resonances are underestimated in these conditions (compared to the B-type one) due to the lower amount of hydroxyl groups in the HA structure. This can explain why we do not observe any strong signal around 166.5 ppm for HA-3 that could confirm the preferential A-type nature of this sample. Moreover, according to Beshah et al.,[47] the strong central resonance that we observe at 168.4 and 168.8 ppm, in HA-2 and HA-3, respectively, could correspond to carbonated amorphous calcium phosphate (ACP). Some recent ^{31}P NMR studies, including ^{1}H-^{31}P CP MAS and ^{31}P-^{31}P spin diffusion experiments, suggest that a nonapatitic calcium-phosphate phase could exist as a disordered layer around the synthetic or natural CHA nanocrystals.[50−52] Furthermore, an amorphous layer of 1−2 nm thickness has been observed through UHR-TEM around some synthetic HA nanocrystals.[53] Thus, the ^{13}C central resonances observed for HA-2 and HA-3 could arise from such a carbonated ACP outer layer. Nevertheless, Babonneau et al. could distinguish in this range two ^{13}C resonances at 168.0 and 169.8 ppm for nanocrystalline CHA synthesized at high temperature that were assigned to other B-type carbonate sites.[48]

For comparison purposes, natural cabonated hydroxyapatite crystals extracted from compact and trabecular bovine bone were studied. To ensure a better spectral resolution in the carbonate region, the organic matrix, mainly collagen, was removed from natural bones by an alkaline treatment as detailed in Experimental Section. The solid state ^{13}C CP MAS spectra of deproteinated compact and trabecular bone are displayed in Figure 7c and d, respectively. Each spectrum shows an asymmetric resonance with a maximum at 170.0 ppm. We can note the similarity with the previous spectra, in particular HA-2, that evidences the incorporation of carbonate anions into HA using our protocol. The main signal at 170.0 ppm shows that the carbonate anions in these natural samples are mainly present in a B-type environment. However, some A-type carbonates are also present in the crystalline structure since a weak shoulder at 166.5 ppm is also observed. Such observations confirm that the predominant substitution in natural apatites appears to be CO_3^{2-} for PO_4^{3-}.[54] Furthermore, the signal around 168 ppm responsible for the asymmetrical shape of the peaks could indicate the presence of a non-negligible proportion of carbonated ACP, which is comparatively less important than in that in our synthetic samples. Overall, our ^{13}C NMR characterization studies strongly suggest that our precipitation process leads to mixed CHA phases where

(47) Beshah, K.; Rey, C.; Glimcher, M. J.; Schimizu, M.; Griffin, R. G. *J. Solid State Chem.* **1990**, *84*, 71–81.
(48) Babonneau, F.; Bonhomme, C.; Hayakawa, S.; Osaka, A. *Mater. Res. Soc. Symp. Proc.* **2007**, *984*, MM06–05.
(49) Mason, H. E.; Kozlowski, A.; Phillips, B. L. *Chem. Mater.* **2008**, *20*, 294–302.
(50) Isobe, T.; Nakamura, S.; Nemoto, R.; Senna, M.; Sfihi, H. *J. Phys. Chem. B* **2002**, *106*, 5169–5176.
(51) Jäger, C.; Welzel, T.; Meyer-Zaika, W.; Epple, M. *Magn. Reson. Chem.* **2006**, *44*, 573–580.
(52) Huang, S.-J.; Tsai, Y.-L.; Lee, Y.-L.; Lin, C. -P.; Chan, J. C. C. *Chem. Mater.* **2009**, *21*, 2583–2585.
(53) Bertinetti, L.; Tampieri, A.; Landi, E.; Ducati, C.; Midgley, P. A.; Coluccia, S.; Martra, G. *J. Phys. Chem. C* **2007**, *111*, 4027–4035.
(54) Elliott, J. C. Calcium Phosphate Biominerals. Phosphates: Geochemical, Geobiological and Materials Importance. *Reviews in Mineralogy and Geochemistry*; Kohn, M. J., Rakovan, J., Hughes, J. M., Eds.; Mineralogical Society of America: Washington, DC, 2002; Vol. *48*, pp 427−453.

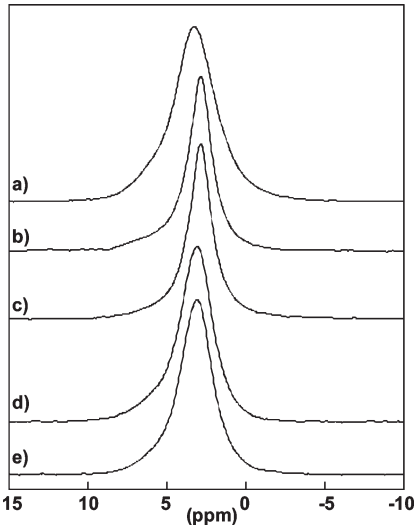

Figure 8. ^{31}P MAS spectra of (a) HA-3, (b) HA-2, (c) HA-1, (d) compact, and (e) trabecular bone.

HA-2 and HA-3 are mainly dominated by a type-B and a type-A carbonate substitution, respectively. We note that such conclusion cannot be drawn unambiguously on the sole basis of FT-IR.

To go deeper into the characterization of our samples, ^{31}P and ^{1}H solid-state NMR studies were performed. The solid-state ^{31}P MAS spectra of HA-1, HA-2, and HA-3 are depicted in Figure 8a,b,c. They display a main resonance at 2.8, 2.8, and 3.2 ppm, respectively, which is characteristic of HA.[55] According to the XRD and TEM studies, the broadness of the resonances, with a total fwhm of 2.3, 2.0, and 3.4 ppm for HA-1, HA-2, and HA-3, respectively, confirms once again the nanocrystalline nature of the HA. The relatively larger broadness of the HA-3 resonance compared to that of HA-1 and HA-2 suggests a more pronounced disorder around the phosphorus atom[56] as a result of the existence of small crystalline domains and vacancies in the structure (the latter are due to the substituted nature of the HA samples), in good agreement with FT-IR data. Furthermore, a significant shoulder at the left foot of the main resonance is observed for HA-2 and HA-3, at 5.6 and 5.7 ppm, respectively. According to previous NMR data obtained through 1D or 2D ^{1}H-^{31}P CP MAS experiments,[50−52] this signal could be related to $HOPO_3^{2-}$ groups that are located in the above-mentioned disordered phase at the nanocrystal surface. In contrast, ^{31}P MAS spectra of both compact (Figure 8d) and trabecular (Figure 8e) bones exhibit identical line shapes (δ = 3.0 ppm and fwhm = 3.0 ppm) indicating similarities between their mineral components for a given bone maturity as previously observed.[57,58]

The ^{1}H MAS NMR spectra of HA-1, HA-2, and HA-3 are depicted in Figure 9a,b,c. Each spectrum presents a

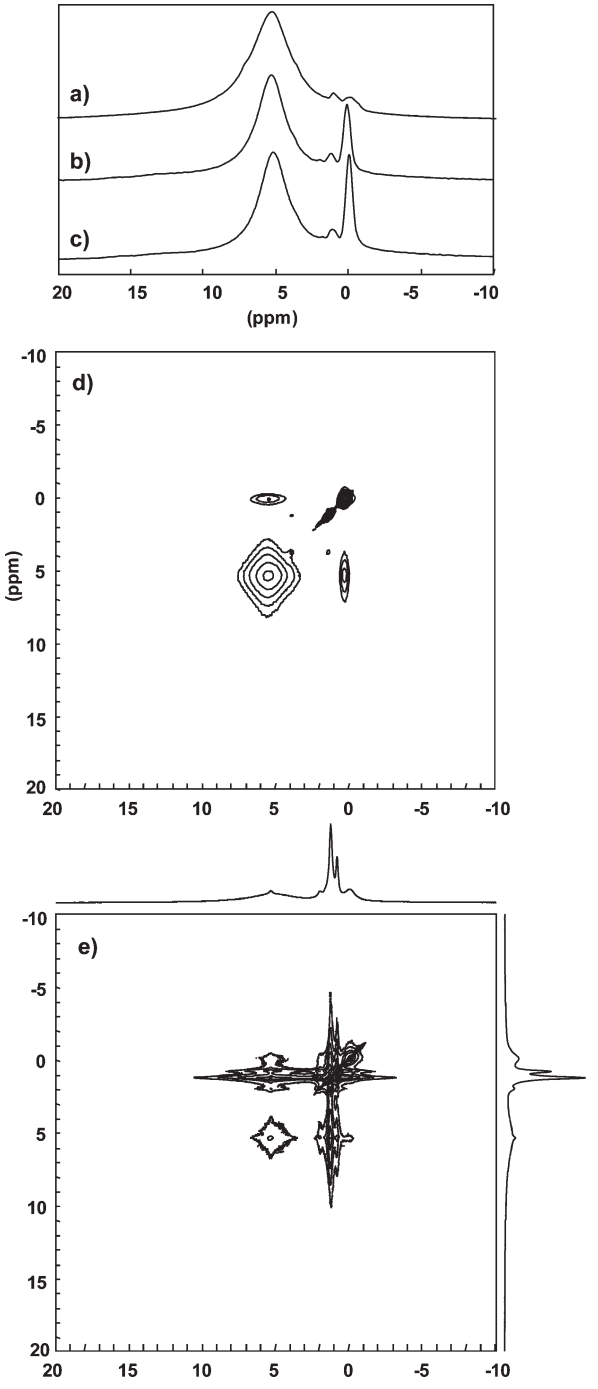

Figure 9. ^{1}H MAS spectra of (a) HA-3, (b) HA-2, and (c) HA-1, and 2D ^{1}H EXSY spectra of (d) HA-2 and (e) compact bone (mixing time = 100 ms).

resonance around 0 ppm characteristic of the HA hydroxyl group.[59] The relative intensity of the OH resonance compared to the H_2O signal is significantly lower for HA-3 compared to that for HA-2. This difference reflects a decrease in the amount of hydroxyl groups in HA-3 due to their substitution by carbonate anions. This result correlates well with FT-IR data and strengthens our identification of HA-3 and HA-2 as mainly type-A and type-B carbonated hydroxyapatite, respectively. The broad resonance at 5.3 ppm is characteristic for adsorbed

(55) Rothwell, W. P.; Waugh, J. S.; Yesinovski, J. P. *J. Am. Chem. Soc.* **1980**, *102*, 2637–2643.
(56) Belton, P. S.; Harris, R. K.; Wilkes, P. J. *J. Phys. Chem. Solids* **1988**, *49*(1), 21–27.
(57) Kolodziejski, W. *Top. Curr. Chem.* **2004**, *246*, 235–270.
(58) Kuhn, L. T.; Grynpas, M. D.; Rey, C. C.; Wu, Y.; Ackerman, J. L.; Glimcher, M. J. *Calcif. Tissue Int.* **2008**, *83*, 146–154.
(59) Yesinovski, J. P.; Eckert, H. *J. Am. Chem. Soc.* **1987**, *109*, 6274–6282.

and structural water. ^{1}H NMR spectra also exhibit a low intensity peak at 1.2 ppm that could be due to the presence of impurities (*vide infra*). Furthermore, weak broad peaks located at 13 and 16 ppm are observed in the HA-2 spectrum. These peaks have already been observed for nanocrystalline HA by different research groups. Isobe et al. assigned them to hydrogen phosphate moieties from monetite.[50] Nevertheless, characteristic ^{31}P resonance of monetite (0.1 and −1.3 ppm) are absent in the corresponding ^{31}P MAS spectrum, and monetite is also not detected by XRD. It was also proposed that these broad peaks correspond to hydrogen phosphate groups located in the disordered outer layer. Indeed, Huang et al. identified it as an ACP-like layer,[52] whereas Jäger et al. suggested the presence of an amorphous phase close to octacalcium phosphate OCP ($Ca_8(HPO_4)_2(PO)_4 \cdot 4H_2O$), thus possessing structural water molecules and POH moieties.[51] This assumption was checked by a 2D ^{1}H exchange spectroscopy EXSY NMR experiment based on the ^{1}H spin diffusion process. This experiment allows one to probe the ^{1}H proximities on a large scale (tens of nanometers) and can thus discriminate structural from adsorbed water molecules. Figure 9d displays the ^{1}H EXSY spectrum obtained with a moderate mixing time (100 ms). A strong exchange peak between OH (0.1 ppm) and H_2O (5.3 ppm) resonances is observed suggesting the presence of these two species in the same nanocrystal and not in separated phases. As concluded by Jäger et al., this result confirms the presence of structural water in the HA nanocrystals. Nevertheless, the presence of an OCP-like phase cannot be confirmed since the 2D ^{1}H spectrum does not evidence any cross-peaks between POH and H_2O signals at any mixing time. For comparison, a 2D ^{1}H EXSY spectrum of compact bone (t_{mix} = 100 ms) is shown in Figure 9e. The apatite hydroxyl resonance is clearly observed at 0 ppm on the F1 and F2 projections together with the fairly broad resonance of water at 5.2 ppm.[60] We can notice that indeed some organic components still remain together with the mineral part since the following resonances at 0.86, 1.26, 2.02, and 5.4 ppm are observed. However, cross-peaks between the water and the hydroxyl resonances can be evidenced as in HA-2. Here, the interpretation is not as straightforward as for the synthetic HA since the water signal correlates with residual signals from the organic matrix. Thus, it can result either (i) from two types of water signing at the same chemical shift, i.e., one in the mineral phase and another in the residual organic phase or (ii) from one type of water molecule located at the interface between both phases (organic/mineral) that would exchange magnetization with the mineral and the residual organic phase. Further investigations are needed in order to confirm this assumption. Thus, the existence and chemical nature of a possible continuous amorphous outer layer remains an open question; in particular, our present HRTEM observations could not evidence this layer, whereas a thin amorphous calcium carbonate layer could be identified in synthetic[61] or natural materials.[62] Instead, we propose that the disordered calcium-phosphate phase associates with the HA nanocrystals as discontinuous small patches. We also note the presence of exchange peaks between the previous unassigned resonance at 1.2 ppm and the small peak at 3.8 ppm. However, these signals do not exhibit any cross-peaks with the HA proton signals. We can safely conclude that these peaks come from a separated impurity. The chemical shifts match well with CH_3 and CH_2 resonances of ethanol, which is used during the washing step and could be adsorbed onto the nanocrystals.

Precipitation Mechanism. The originality of the present route to nanocrystalline hydroxyapatite comes from the fact that neutralization starts at a very low initial pH (2.2), in contrast with the usual methods that mainly involve alkaline precursor solutions to avoid the precipitation of other calcium-phosphate phases.

Here, the continued diffusion and solvation of NH_3 into the solution leads to a pH gradient in the reaction vessel from top to bottom. Indeed, ammonia ($pK_a(NH_4^+/NH_3) = 9.25$) dissolves and diffuses into the salts solution leading to an increase in pH ($pH_i = 2.2$; $pH_f = \sim 10$). During alkalinization, a critical pH value is reached where the nucleation is triggered. According to previous results in the literature for calcium carbonate precipitation,[20] the vapor diffusion method is known for slow crystallization. It allows a thermodynamic control of the growth/crystallization process so that the thermodynamic phase, i.e., HA, was expected to be obtained preferentially here. However, another feature of the vapor diffusion process is that the resulting products are highly dependent on the experimental setup.[63,64] We took advantage of this to clarify the course of our process, by performing the following variations in the experimental procedure: (i) For similar concentrations and volume, the use of a larger vessel but 10 times smaller in height (5 mm) than the reference conditions (50 mm) led to the additional formation of brushite crystals, $CaHPO_4 \cdot 2H_2O$ (DCPD) in the precipitation media, whereas the final pH was unchanged. In these conditions, the pH gradient is smaller, and the time to reach the critical pH for precipitation is faster (kinetic control). Thus, the precipitation should be less selective, hindering the crystallization of the sole HA crystalline phase. (ii) For similar setup conditions where only the initial NH_3 quantity is decreased in the closed chamber, the final pH is lower (5−7), leading also to brushite formation. Such observations are in agreement with previous results in the literature showing that brushite formation starts at lower pH than HA and is described as the more stable phase at pH < 4.2.[11,12] On this basis, it is clear that both the

(60) Cho, G.; Wu, Y.; Ackerman, J. L. *Science* **2003**, *300*, 1123–1127.
(61) Nassif, N.; Pinna, N.; Gehrke, N.; Shirshova, N.; Tauer, K.; Antonietti, M.; Cölfen, H. *Angew. Chem., Int. Ed.* **2005**, *117*, 6158–6163.
(62) Nassif, N.; Pinna, N.; Gehrke, N.; Antonietti, M.; Jäger, C.; Cölfen, H. *Proc. Natl. Acad. Sci. U.S.A.* **2005**, *102*, 12653–12655.
(63) Gehrke, N.; Cölfen, H.; Pinna, N.; Antonietti, M.; Nassif, N. *Cryst. Growth Des.* **2005**, *5*, 1317–1319.
(64) Neira, A.; Fernandez, M. S.; Reteurt, J.; Arias, J. L. *Mater. Res. Soc. Symp. Proc.* **2004**, *EXS-1*, H6.18.11.

Scheme 2. Proposed Precipitation Mechanisms of Type-A and Type-B CHA in the One-Pot Aqueous Synthesis[a]

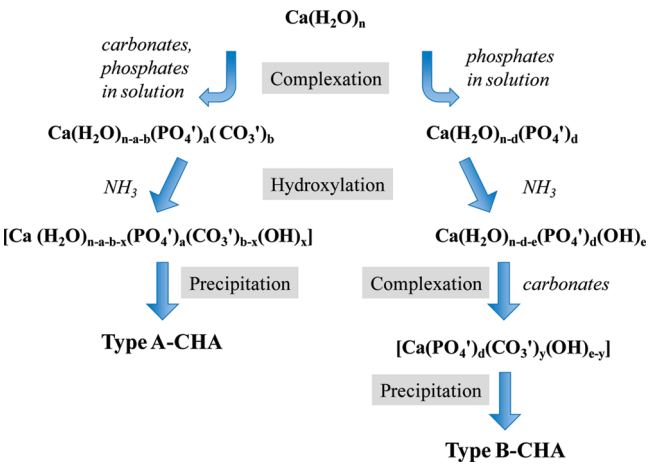

[a] $PO_4' = H_2PO_4^-$ or/and HPO_4^{2-} or/and PO_4^{3-}.

quantity of ammonia and the vessel geometry are of primary importance to establish a suitable pH gradient that allows the sole precipitation of crystalline HA.

A further question then arises on the influence of the carbonate precursor nature on the type of carbonate substitution occurring in the apatite structure. It was suggested that the physical form (i.e., gas or solvated ions) of the carbonate source has a direct impact on the precipitation reaction. Indeed, synthetic A-type carbonated apatite can be prepared by heating HA in CO_2 atmosphere, whereas B-type carbonated apatite powders are generally synthesized from a precipitation reaction in aqueous media.[42] Another important parameter is the presence of ammonium and sodium ions that were found to favor the formation of B-type structures by Ca^{2+} substitutions.[65,66]

In aqueous solution, calcium ion forms aqueous complexes $Ca(H_2O)_n^{2+}$; when phosphates are present in solution, calcium-phosphate complexes such as $[Ca(H_2PO_4)_x]\cdot(H_20)_{6-x}^{(2-x)+}$, $[Ca(HPO_4)_x]\cdot(H_20)_{6-x}^{(2-2x)+}$, or $[Ca(PO_4)_x]\cdot(H_20)_{6-x}^{(2-3x)+}$ should exist in the reaction media, as a function of pH (Scheme 2).

When carbonate ions are directly added to the solution (i.e., before alkalinization), calcium-carbonate complexes should be negligible compared to the phosphate ones (following the pK_a of the carbonate ($pka_2(H_2CO_3) = 6.3$ and $pka_1(H_2CO_3) = 10.1$) and phosphate ($pK_{a3}(H_3PO_4) = 2$, $pK_{a2}(H_3PO_4) = 6.9$,a nd $pK_{a1}(H_3PO_4) = 11.7$) species). However, mixed calcium−phosphate−carbonate complexes may pre-exist, where carbonates and phosphates are in competition for Ca^{2+} binding. When the number of hydroxyl groups increases in solution through the addition of the NH_3, zero-charged mixed complexes form, allowing the precipitation of a phase where carbonates substitute phosphate groups as the major phase, i.e., the B-type of CHA. In contrast, the thermal decomposition of ammonium carbonate leads to the slow generation of NH_3 and CO_2. First, the pH increases steadily due to ammonia, which favors then the dissolution of carbon dioxide into the solution. Compared to the previous case, calcium−phosphate−carbonate mixed complexes are not initially present in the precursors solution. This means that the first hydroxylation reaction should predominantly occur on calcium-phosphate complexes. Then, carbonates (CO_3^{2-}) and more likely hydrogenocarbonates (HCO_3^-) ($pK_{a1} = 10.1$) would react on the most basic part of the complex, i.e., the hydroxyl group. Finally, substitution of the hydroxyl groups followed by the formation of this new carbonated complex would lead preferentially to the precipitation of the A-CHA.

4. Conclusions

The present work finds its inspiration from *in vivo* conditions and shows that *in vitro* synthesis of biomimetic apatite can be set by using simple biological parameters. We have setup a one step process for the formation of nanocrystalline hydroxyapatite in aqueous medium, at room temperature, starting with acidic salt precursors. Moreover, this procedure can be easily extended to the incorporation of other elements or groups such as carbonate ions within the apatite structure. Very interestingly, the process is also compatible with the mineralization of delicate organic compounds such as collagen.[67] The obtained apatite nanocrystals exhibit a morphology, crystallite size, and Ca/P molar ratio very close to those of mature bovine bone. Additionally, a better similarity between the synthetic and the natural HA was obtained when using an aqueous carbonate precursor (vs gas precursors), which makes sense since it occurs in that way *in vivo*.

Thus, we could note that different kinds of carbonated compounds, characterized as single B- or A-CHA type by FT-IR, in fact possess different carbonate substitution types in their structure that can be clearly distinguished through their respective ^1H and ^{13}C MAS spectra.

Acknowledgment. We thank J. Maquet for help in the NMR studies, D. Jalabert and P. Legriel for help in the TEM studies. We are grateful to J.P. Jolivet, C. Sassoye, E. Belamie, F. Babonneau and C. Gervais for their scientific help. T. Azaïs acknowledges the Young Researcher ANR grant NanoBioMat n° 06-JCJC-0089 for financial support.

Supporting Information Available: XRD patterns of HA-2, HA-3, deproteinated compact and trabecular bovine bone, SEM image and XRD pattern of HA-4, and FT-IR spectra of HA-1, HA-2, and HA-3 (PDF). This material is available free of charge via the Internet at http://pubs.acs.org.

(65) Vignoles, M.; Bonel, G.; Holcomb, D. W.; Young, R. A. *Calcif. Tissue Int.* **1988**, *43*, 33–40.
(66) Peroos, S.; Du, Z.; de Leeuw, N. H. *Biomaterials* **2006**, *27*, 2150–2161.
(67) Nassif, N.; Gobeaux, F.; Seto, J.; Belamie, E.; Davidson, P.; Panine, P.; Mosser, G.; Fratzl, P.; Giraud-Guille, M.-M. *Chem. Mater.* **2010**, DOI:10.1021/cm903594n.